International Journal of
Turbomachinery
Propulsion and Power

MDPI

Article

Impact of the Exhaust Geometry on Flow Losses in a High-Pressure Steam Turbine †

Christian Musch *, Simon Hecker, Daniel Gloss and Ruben Steinhoff

Siemens AG, Rheinstraße 100, 45472 Mülheim an der Ruhr, Germany; simon.hecker@siemens.com (S.H.); daniel.gloss@siemens.com (D.G.); steinhoff@ift.uni-hannover.de (R.S.)

* Correspondence: christian.musch@siemens.com

† This paper is an extended version of our paper published in Proceedings of the European Turbomachinery Conference ETC'11, 2015, Paper No. 138.

Academic Editor: Marcello Manna
Received: 14 September 2016; Accepted: 18 October 2016; Published: 9 November 2016

Abstract: The design of modern steam turbines for power plant applications is steering towards higher efficiencies. A considerable contribution to this aim is expected from a reduction of flow losses in turbine intakes and exhausts. The present study therefore deals with the optimisation of the exhaust of a high-pressure (HP) turbine. In the first part of this study a numerical model is presented which allows for a precise representation of the exhaust flow. This computational fluid dynamics (CFD) model has been validated with a fair amount of experimental data from a test rig. For the second part of the study comprehensive numerical investigations have been carried out, considering the major geometrical parameters of such a geometry. In order to minimize the effort in design time and preprocessing a fully parametric 3D model of the geometry is created to prepare the different design variations. The results of these simulations allow to assess the performance differences of given exhaust designs in the early design phase without the need for expensive CFD simulations. Finally a potential for improvement of 300 kW for a 800 MW power plant is shown by means of a comparison of an optimised design to the baseline geometry.

Keywords: steam turbine; exhaust flow; volute design

1. Introduction

Besides the effort to further increase the efficiency of modern steam turbine power plants, the design of the turbine is also driven by a demand to reduce costs. A major factor for the overall costs of the turbine is the installation size of the turbine. Mostly, a size reduction will be in conflict with the reduction of flow losses. A more thorough look at the flow is therefore becoming more and more essential to avoid unnecessary flow losses and efficiency penalties. The exhaust area of a turbine is significant for the overall size of each turbine as the specific volume of the steam and hence the volume of the flow passage increases from turbine inlet to outlet. By trying to reduce the size of the turbine it is not unlikely that existing design rules will be violated. The basic design of a high-pressure turbine exhaust is shown in Figure 1. Although the design of the turbine itself is rather different for the different steam turbine manufacturers, the design of the exhaust is rather similar. The design consists of an axial-radial diffuser to recover some of the kinetic energy and hence reduce the inlet velocity to the ring chamber which is responsible to collect the steam and guide it to the successive piping. In all those designs, a vortex will form in the exhaust ring chamber which is a major source for flow losses. Some of the main influence parameters on the flow losses between the last HP turbine stage and the adjacent pipe work of a typical high-pressure (HP) turbine exhaust are analyzed in this paper.

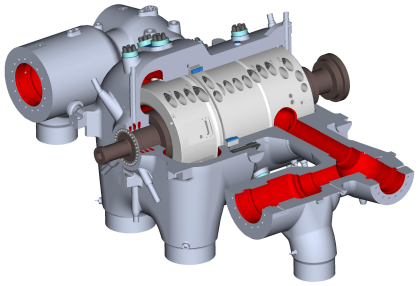

Figure 1. Image of a typical high-pressure (HP) turbine.

Literature Survey

So far, the amount of publications dealing with the exhaust area of a HP turbine are very rare. The best known or most common description is given by Traupel [1]. Moreover, Hausenblas [2] performed detailed measurements at a turbine exhaust with a geometry similar to a typical HP turbine. A drawing of the baseline design of his investigations can be seen in Figure 2. In addition to showing the performance impact of the diffuser, he also showed that the geometry of the exhaust chamber has a significant influence on the overall losses. In the improved design the losses could be reduced by roughly 35% compared to the baseline. Besides these publications, it is mainly literature on compressor volutes that gives hints for a geometric similar design. The flow topology in the exhaust ring chamber is quite similar to that of a compressor volute so that some basic geometric influence parameters can be deduced. As the exhaust volute of a compressor is essential for the overall behaviour of the compressor a large amount of publications dealing with this topic can be found.

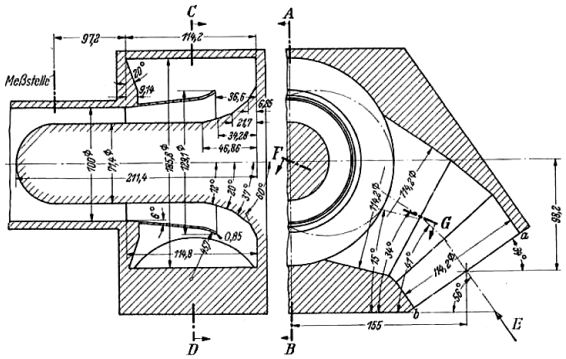

Figure 2. Exhaust model investigated by Hausenblas [2].

Investigations by Hübl [3] for a volute with circular cross section show that a tangential inlet to the ring chamber results in a better compressor efficiency (see Figure 3). In the experiments of Lendorff and Meienberg [4] a similar behaviour could be observed.

Mishina and Gyobu [5] studied the influence of different cross sections of the volute on the flow losses. They reasoned that a circular cross section has the lowest flow losses. Also, the radial location of the volute has a major influence on flow losses. They showed that although the cross section has the same area the volute with the smaller radius has higher losses. Stiefel [6] came to the same results from his measurements. Ayder [7] argues that this is due to a re-acceleration of the fluid resulting from the reduction of the radius. This in turn reverses some of the pressure rise achieved in the diffuser. Furthermore Ayder [7] reports that a quadratic cross section is advantageous as the fluid in the ring chamber vortex is not accelerated and decelerated with every revolution. On the contrary Brown and Bradshaw [8] performed measurements for four double volutes with different cross-sectional shapes. They argue that neither the inlet position to the volute nor the form of the cross section have a significant influence on the compressor performance. However, Yang et al. [9]

analyzed four different types of cross-section shapes with symmetric inlet and found a round shape to give the highest pump efficiency. Reunanen [10] claims that the shape of the cross section is of minor importance as the tangential velocity is much higher compared to the radial velocity. However, this is not necessarily true for a turbine exhaust.

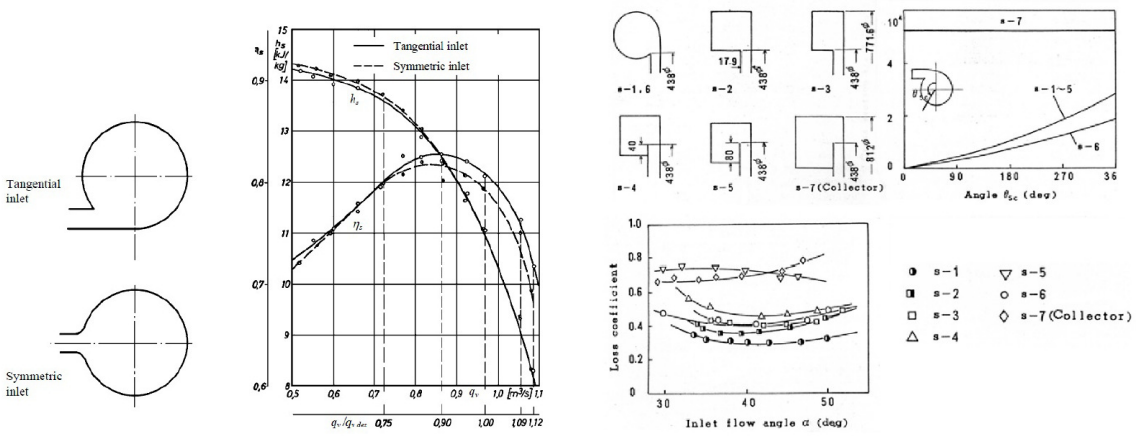

(**a**) (**b**)

Figure 3. Influence of ring chamber geometry on compressor performance. (**a**) Influence of inlet position acc. to Hübl [3]; (**b**) Influence of cross section acc. to Mishina et al. [5].

2. Results

2.1. Validation of Numerical Model

In this section a numerical model is presented which is validated with the help of test rig measurements. In the first part the test rig will be introduced briefly and in the following sections the influence of mesh size and turbulence modeling will be discussed.

2.1.1. Test Rig

Measurements were conducted by Urban [11] in the late 1990's. A scaled plexiglas model has been investigated, which is similar to an actual HP turbine exhaust. Figure 4 shows a photography of the model. The geometry of the cross section as well as the circumferential design are shown in Figure 5. It can be seen that the model features two exhaust ports and a constant annular cross section around the circumference. Furthermore, the different measurement planes can be identified. Pressure taps for static pressure measurements have been installed in the inlet of the test rig as well as in plane 0 and plane 1. Plane 0 and plane 1 are the diffuser inlet and diffuser outlet plane respectively. As can be seen in Figure 5 measurements have been conducted in these planes at eight different positions around the circumference. Stagnation pressure has been measured at the same locations and additionally in the outlet flange to determine the overall flow losses. For this purpose a five hole wedge type probe has been traversed at these locations. Hence, beside the stagnation pressure the complete velocity vector has been determined along the channel span. The test rig has been driven by a compressor and exhausts to ambient. A perforated metal sheet at the inlet has been used to model the upstream turbine stages. Similar to a real turbine it creates a rather homogeneous mass flow and total pressure field around the circumference. This has further been accompanied by 24 flow guides in the inlet section to suppress any tangential velocity field. The test rig could be equipped with different diffuser designs. Two of these have been used for the validation. The first diffuser has a very moderate area ratio of 1.2 showing no flow separation within the diffuser. The second one is a bit more aggressive with an area ratio of 1.6 showing considerable flow separation.

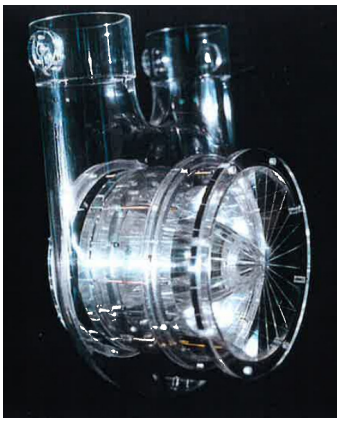

Figure 4. Image of test rig taken from Urban [11].

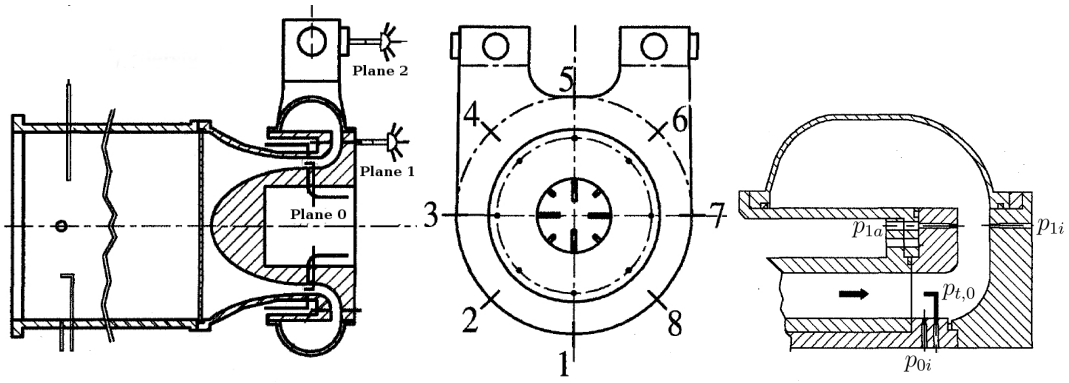

Figure 5. Test rig geometry and measurement locations acc. to Urban [11].

2.1.2. Numerical Model Part 1

The numerical simulations carried out in this study are conducted with the commercial software code ANSYS CFX. Steady state as well as transient simulations are done to determine the flow losses for the different geometries. Spatial discretization is done using a high resolution scheme, resulting in almost second order accuracy. For all transient simulations a temporal discretization using an implicit second order Euler scheme is employed. Turbulence closure is done with an eddy viscosity approach based on the Reynolds-Averaged Navier-Stokes equations. For the validation of the numerical model different turbulence models have been investigated. Besides the turbulence models, the mesh size is also investigated. In order to allow for an automated grid generation, an unstructured tetrahedral meshing approach is used. Additional inflation layers (using prism elements) next to all solid walls are utilized to accurately calculate the boundary layers. Figure 6 shows a typical mesh of the computational domain. Fluid properties have been modeled using an ideal gas assumption for the simulation of the air driven test rig. The flow domain of test rig is modeled starting upstream of the perforated metal sheet and ending at the exhaust ports. The perforated metal is modeled as a porous medium with a linear loss characteristics. The loss coefficient is calculated according to Equation (1) to reflect the measured pressure loss.

$$k_{\text{loss}} = \frac{\Delta p_{t,\text{plate}}}{b\frac{\varrho}{2}c^2} \tag{1}$$

with b, ϱ and c being the metal sheet width, the fluid density and the flow velocity, respectively. The pressure loss across the metal sheet is roughly one order of magnitude higher than the losses of the exhaust itself. As a boundary condition at the inlet the stagnation pressure and temperature are used. As outlet boundary condition the mass flow is prescribed.

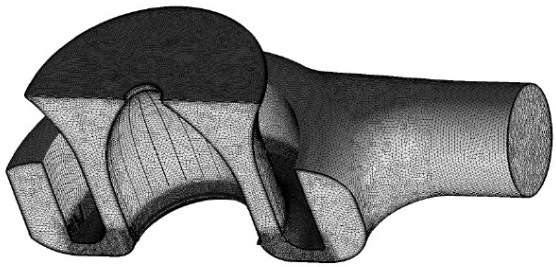

Figure 6. Symmetric mesh of test rig model.

2.1.3. Mesh Sensitivity and Model Inaccuracy

In a first set of simulations, the sensitivity towards mesh resolution is investigated. The $k-\omega$ turbulence model is used for the presented results. The global mesh size and the boundary layer resolution are varied separately and the results are analyzed with regard to overall pressure loss. To minimize the computational effort at this stage of the study it is thought to be reasonable to exploit the symmetry of the model, i.e., only one half of the test rig is modeled in computational fluid dynamics (CFD). The results gained in this study are shown in Table 1. The loss coefficients are normalized with the value of mesh 4. Based on this study a grid resolution according to the mesh parameters used in mesh 4 is found to be sufficient for an accurate (below 3% difference to the finest investigated mesh) representation of the flow losses.

Table 1. Data of mesh study.

	Mesh 1	**Mesh 2**	**Mesh 3**	**Mesh 4**	**Mesh 5**	**Mesh 6**
Mesh size (Node Count)	4 mio	3 mio	3 mio	2.5 mio	2.5 mio	2 mio
Boundary Layer Resolution (y^+_{max})	10.0	10.1	5.3	9.9	10.0	19.0
Number of Prism Layers	30	23	23	23	19	15
Normalized Loss Coefficient ζ_{norm}	0.976	0.988	1.008	1.000	0.984	0.869

As a further proof, the flow profiles gained from meshes 1 and 4 are compared to each other. Figure 7a,b show the velocity profiles corresponding to measurement plane 1 (i.e., diffuser outlet) for positions 1 and 5. The definitions of the flow directions as used in the measurements are shown in Figure 8. Although some differences could be observed in the flow profiles for the two meshes the discrepancy to the measurements is even more noticeable. This of course can be attributed to the symmetry boundary condition used in the CFD, which constricts the flow in an unrealistic way.

Consequently, a simulation using a full model has to be carried out. However, due to the additional degree of freedom the flow becomes rather unsteady in these regions and a converged steady state solution is hard to find. Taking a closer look at the flow field this behaviour can be explained by oscillations in the stagnation points at positions 1 and 5.

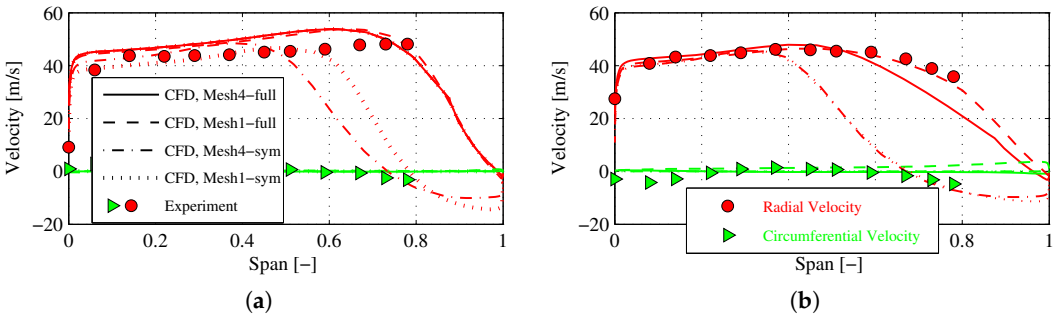

Figure 7. Velocity profiles at diffuser outlet/Mesh sensitivity and model errors. (**a**) Pos.1; (**b**) Pos.5.

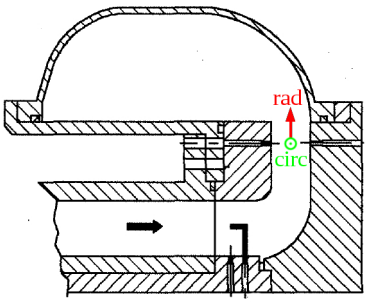

Figure 8. Flow directions at diffuser outlet.

These stagnation points shift from left to right around the circumference as indicated in Figure 9, which shows an instantaneous streamline plot of the exhaust flow. Thus, a transient simulation must be carried out to correctly predict the whole flow field. In order to minimize the computational effort it is first of all investigated how the time step of the simulation influences the results. Primarily this is done in order to determine the largest possible time step.

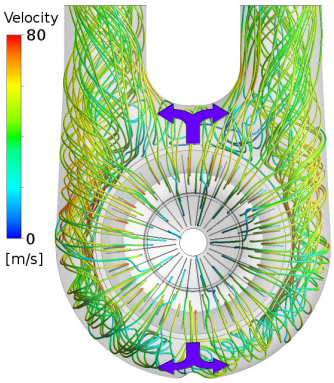

Figure 9. Streamline plot of the exhaust flow field.

To be able to transfer the results to other geometries a global Courant number is introduced. In Equation (2), variables d,c and Δt denote the ring chamber diameter, the average flow velocity and the actual time step of the simulation.

$$\mathrm{CFL}_{\mathrm{global}} = \frac{c\Delta t}{d} \tag{2}$$

From Figure 10 it can be seen that up to a value of $\mathrm{CFL}_{\mathrm{global}} = 0.2$ there is hardly any change to the calculated pressure losses. The corresponding time step will thus be used further on. Also all further simulations described in Section 2.2 are carried out accordingly.

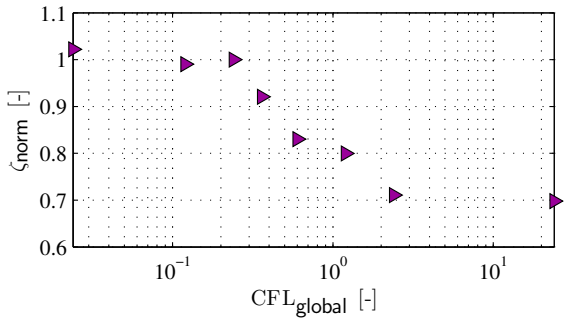

Figure 10. Influence of time step on pressure loss.

2.1.4. Turbulence Modeling

The usual suspects for this kind of flow study (i.e., the $k-\varepsilon$, $k-\omega$ and Shear Stress Transport (SST) turbulence model) have been analyzed. The local flow fields in measurement planes 0,1 and 2 are used to assess the performance of the different turbulence models. The first results presented are for the moderately opening diffuser geometry named model 1 further on. The pressure distribution around the circumference in the diffuser inlet (plane 0) is presented in Figure 11a. Positions 1 and 5 correspond to peripheral angles of $-180°/180°$ and $0°$, respectively (compare Figure 5).

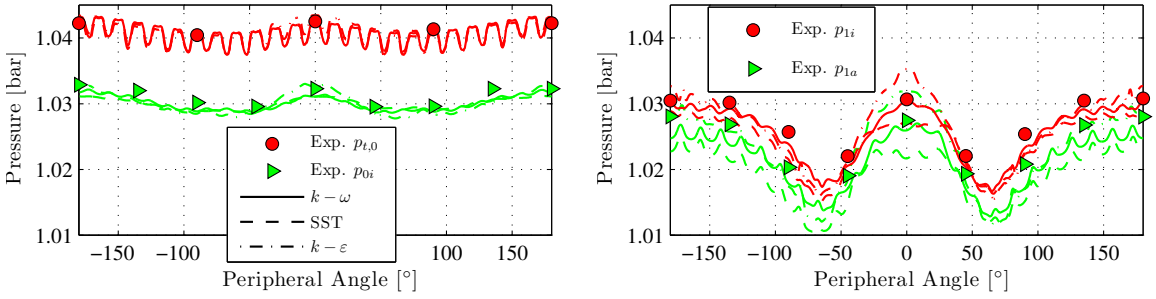

Figure 11. Pressure distribution at diffuser inlet and outlet for model 1. (**a**) Diffuser inlet; (**b**) Diffuser outlet.

A good correlation to the measurement can be found. This indicates that the boundary conditions in the CFD are chosen correctly. The pressure distribution at the outlet shows some differences between the models. The $k-\varepsilon$ and the $k-\omega$ model match the measurements reasonably well, whereas the SST model predicts a lower diffuser outlet pressure, indicating that either flow separation occurs or the flow losses are over predicted by the SST model. It should be noted, that the wiggles in Figure 11b are caused by the wakes of the 24 flow guides in the inlet section. Figure 12a–d show profiles of the transient time averaged velocity components along the span in the diffuser outlet at different circumferential positions. For the definition of the flow directions see Figure 8. Only the results of one half of the model are plotted here, as the second half shows basically the same trends. For all models an overall good correlation to the measurements can be observed, except for position 5. The SST and the $k-\varepsilon$ model are a bit more off the experimental data whereas the $k-\omega$ model seems to be superior to the former ones. At this position a large vortex can be found in the simulations (see Figure 9). This region is also one of the main contributors to the unsteady behaviour of the flow. The $k-\omega$ model is the only model to correctly predict the flow field at this location. In Figure 13a,b the velocity profiles in the exhaust ports are presented. Again, due to the flow symmetry only the results of one half of the model are shown. Definitions of the velocity components are again corresponding to the ones shown in Figure 14. One has to be aware that the steps in the radial and circumferential velocity profiles are a result of these

conventions. Also for this position a rather good agreement between simulation and experimental data can be found. It has to be noted though, that the SST model predicts a wrong trend on the radial velocity on Line 4. This is due to the fact that in the simulation with the SST model the vortex center is a little bit shifted to the side compared to the other simulations and to the measurement. So far it can be stated that for a non-separating diffuser flow the general flow field is predicted sufficiently correct by all models.

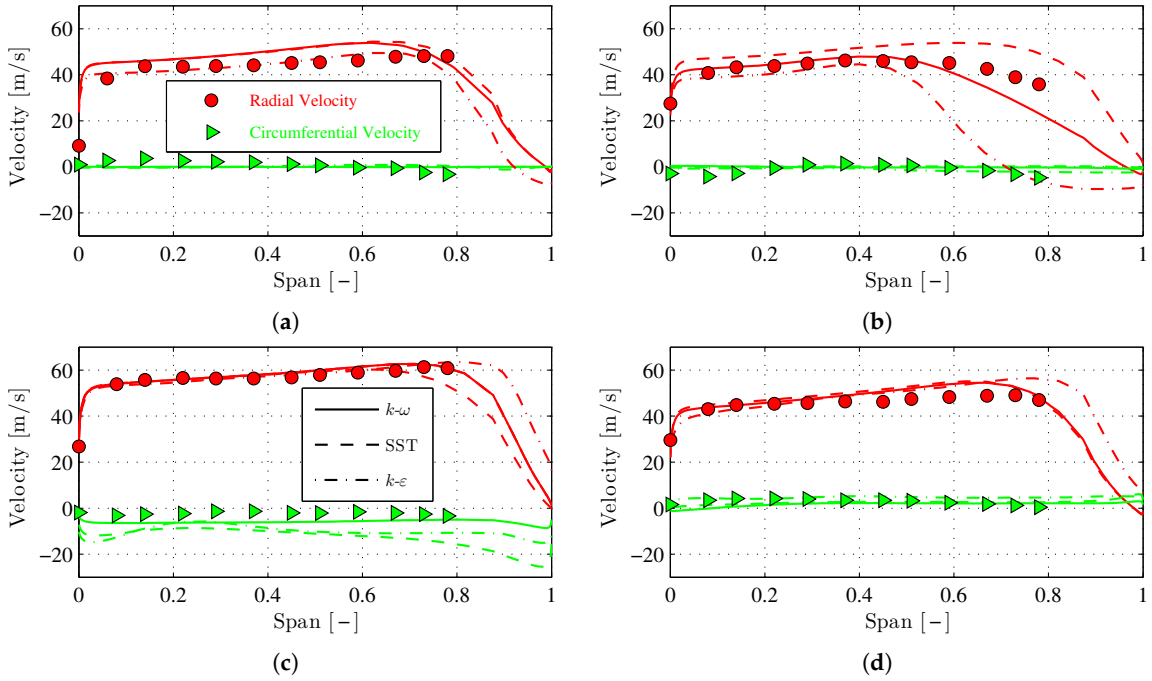

Figure 12. Velocity profiles at diffuser outlet for model 1. (**a**) Pos.1; (**b**) Pos.5; (**c**) Pos.6; (**d**) Pos.8.

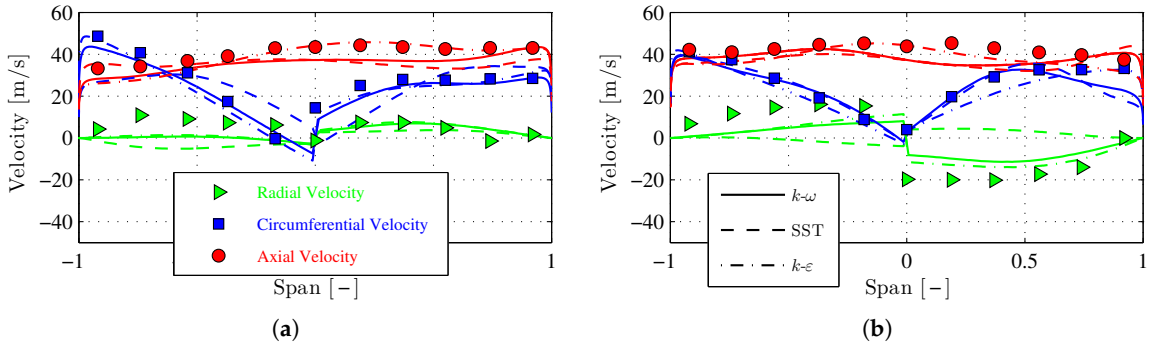

Figure 13. Velocity profiles at exhaust port for model 1. (**a**) Line 3; (**b**) Line 4.

The results of the second diffuser configuration which is investigated are shown in the Appendix. Again, the velocity profiles at the diffuser outlet and exhaust port are shown in Figures A1a–A2b. In this investigation only two turbulence models have been used. As before, the two models show a good correlation to the measurements. Also the flow separation and the recirculation zone are predicted quiet accurate. As a resume of the results presented so far, it can be stated that all turbulence models are capable to predict the time average flow field good enough for the purposes of this paper. Ultimately, the $k-\omega$ model is chosen for all further investigations as it showed slightly better results in comparison to the experiments.

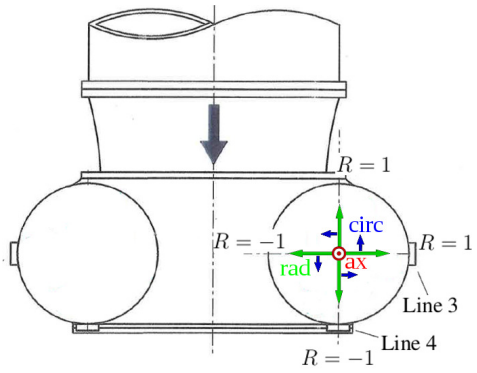

Figure 14. Flow directions at exhaust port.

2.2. Parameter Study

For this part of the paper a parametric model of the exhaust has been created. The geometry is a generic model of a typical barrel type HP turbine. Parameters which have been investigated are the aspect ratio of the exhaust ring chamber cross-section, the corner radii of the chamber and the wall angles. The influence of all these parameters on the overall pressure loss Δp_t is evaluated by means of a normalized pressure loss coefficient, which yields the definition for ζ_{norm} shown in Equation (3).

$$\zeta_{\text{norm}} = \frac{\Delta p_t}{\Delta p_{t,\text{baseline}}} \tag{3}$$

Figure 15 shows a 3D model of the exhaust with the stator vane and rotor blades as well as the parameters of the ring chamber cross section.

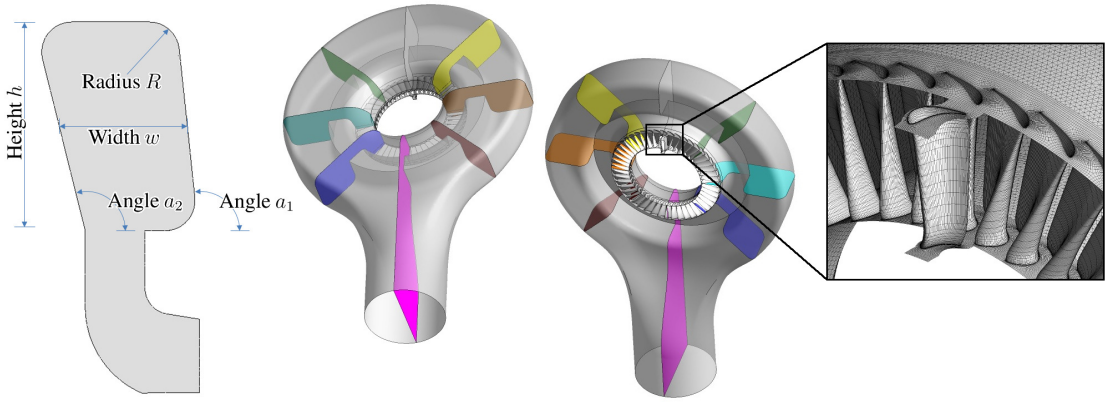

Figure 15. Numerical setup for parameter study.

The ring chamber has a constant cross section between sections 6-7-8-1-2-3-4 (as defined in Figure 5). The baseline design which is shown in Figure 15 in the 3D view is furthermore characterized by a quadratic cross section with 90° wall angles. The corner radii have a size of $R = 80$ mm and the area of the constant part of the ring chamber as shown in Figure 15 is defined by a ratio of $AR = 0.75$ with reference to the exhaust port area.

2.2.1. Numerical Model Part 2

In order to correctly predict the flow losses it is important that the flow entering the exhaust chamber is as close as possible to the actual inflow conditions of the turbine. This is ensured in the present study by including the last stator and rotor row of the turbine in the CFD model. As the

exhaust geometry is not symmetric around the circumference, also the flow field will vary accordingly. To account for that, all blades of the last rotor row are modeled. The stator vane and the rotor blade are connected via a Mixing-Plane- (or Stage-) Interface. The rotor domain is connected to the exhaust domain using a transient rotor-stator (or sliding mesh) interface. As inlet boundary conditions the mass flow and total temperature are applied. At the outlet, the static pressure is prescribed. Fluid properties are taken from a steam table according to IAPWS-IF97. Although the mesh of the blade and vane are chosen to be very coarse the overall node count adds up to roughly 7.5 Mio. nodes. All flow fields shown in the following sections are time-averaged plots.

2.2.2. Corner Radii

In the first part of the study the influence of the corner radii on the flow field is investigated. Therefore, four different radii are analyzed with an otherwise unchanged geometry. It can be shown that the flow losses are increasing as the radius is increased. This can be explained when taking a look at the flow field in the ring chamber. Figure 16 shows the tangential velocity and the corresponding pressure field normalized by the inlet pressure in a horizontal cut plane (see Figure 15) for the investigated geometries.

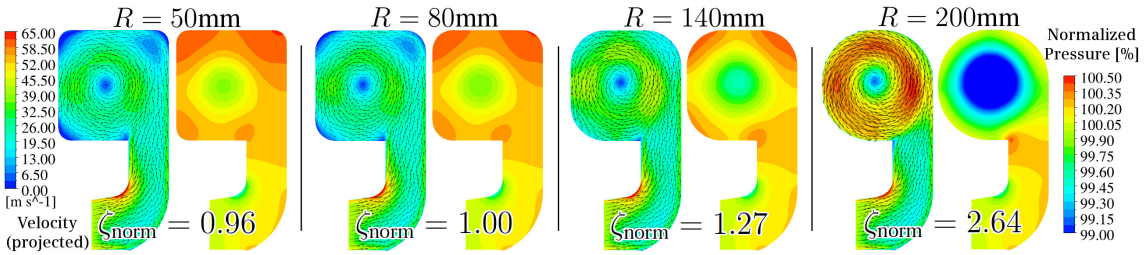

Figure 16. Velocity and pressure fields for different corner radii.

It can be seen that with a larger radius also the flow velocity gets higher. Due to the higher flow velocity it is apparent that the losses are likewise increasing. This however can be further explained from the contour plots of the pressure at the corresponding position. In these contour plots the pressure can be found to be high in the corners of the chamber as a result of flow stagnation in the corners. This pressure increase leads to a decrease of the rotational velocity of the vortex and thus to a decrease of friction losses. This is indeed a known feature from labyrinth seals. Kuwamura et al. [12] for example showed that a stepped labyrinth seal with a circular shaped cavity has a smaller leakage flow than a rectangular shaped cavity due to an enhanced vortex velocity. Furthermore it can be seen that an asymptotic behaviour exists. Once the radius goes below a certain value the pressure field does not change markedly and thus also the losses are almost constant. The baseline design therefore already has a reasonable size with respect to aerodynamic considerations.

2.2.3. Wall Angle

The next parameters investigated are the wall angles a_1 and a_2. Figure 17 shows the flow fields of four different geometries, which have been simulated. Angles of 75° and 105° have been considered in the CFD for both sides. The influence of angle a_1 on the overall pressure loss is hardly visible. Accordingly, only a minor influence on the rotational velocity can be determined as shown in Figure 17. It can thus be deduced that the drag forces in the corners are not markedly raised by changing wall angle a_1. However, by changing angle a_2 a reasonable change in the pressure losses can be identified. For an angle of $a_2 = 105°$ a slight reduction of the overall losses can be observed. From the pressure plot shown in Figure 17 for this configuration a steeper pressure rise along the angled wall is perceptible when compared to the baseline design in Figure 16. This can be attributed to an additional diffusion due to the inclined wall. Also the size of the ring vortex is reduced in this setup

which as well contributes to the decreased losses. Taking a look at the configuration with $a_2 = 75°$ an opposing effect can be seen, which is even more prominent. In this case the flow is accelerated rather than decelerated resulting in a higher rotational velocity and therefore a higher pressure loss. A bent in this direction should therefore be avoided if possible.

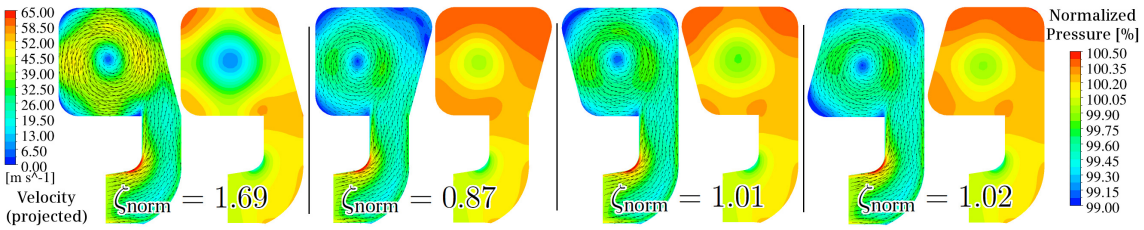

Figure 17. Velocity and pressure fields for different wall angles.

2.2.4. Aspect Ratio

The next parameter that is varied is the aspect ratio of the ring chamber. In all seven different configurations have been investigated. The flow field in the horizontal cut plane is again used to visualize the flow topology. Figure 18 shows the results for those simulations.

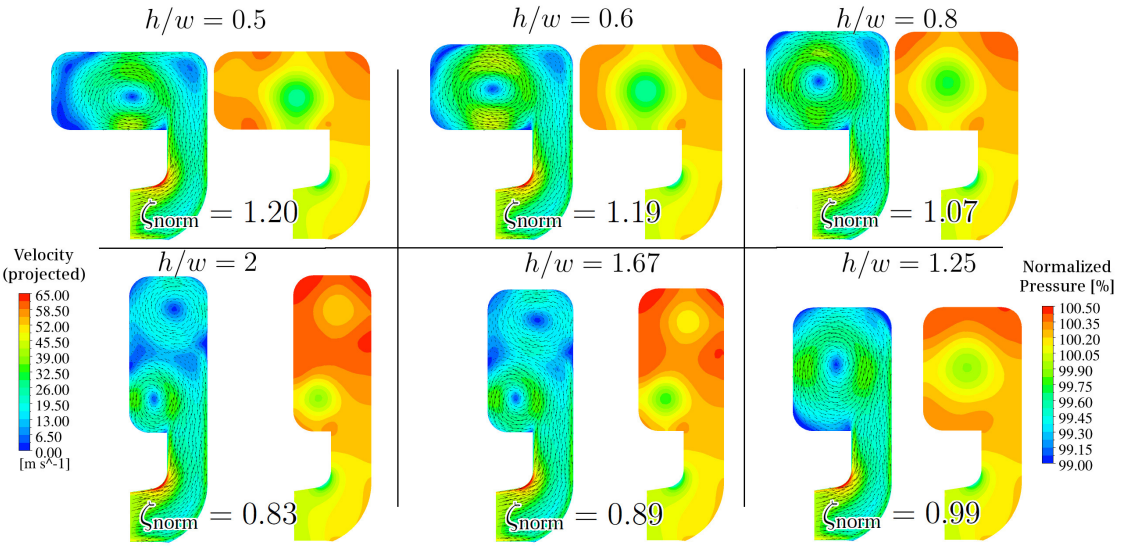

Figure 18. Velocity and pressure fields for different aspect ratios.

As apparent from the rotational velocity of the chamber vortex, in general the flow losses decrease from small to large aspect ratio. Taking a closer look at the different results it can be seen that for very large aspect ratios an additional counter-rotating ring vortex is formed,resulting in two smaller vortices. This reduces the losses furthermore as on the one hand the lower vortex (with high rotational velocity) is small and thus the losses attributed to this vortex are likewise small. On the other hand the upper vortex has a very low rotational velocity due to a strong diffusion of the flow field between both vortices. In general a larger chamber radius is advantageous due to additional flow deceleration caused by an increased flow area resulting from the larger radius. This has also been pointed out by Steglich [13] in their study on different compressor volutes. For small aspect ratios the formation of a second vortex can hardly be found. Only for the smallest aspect ratio considered in this study a very small counter-rotating vortex can be identified. For this configuration indeed the rotational velocity of the vortices is indeed reduced compared to the case with $h/w = 0.6$. However, the overall losses are still on the same level as the flow losses created in the transition from the ring chamber to the exhaust port are increasing with smaller aspect ratios.

2.2.5. Optimised Design

Finally, a combination of the design features formerly analyzed is investigated. Thus, a configuration with corner radii of $R = 80$ mm, an aspect ratio of $h/w = 2$ and inclined sidewalls with angles of $a_1 = 80°$ and $a_2 = 105°$ is created. The flow field, i.e., velocity and pressure distribution, is shown in Figure 19. As can be seen the rotational velocity of the ring vortex is very small due to the large aspect ratio, the small corner radii and the increased angle a_2. The second sidewall also features a reasonable inclination. This is done to avoid the formation of a second vortex which could be identified for all designs with a large ascpect ratio as shown in the former section. The combination results in a significant reduction of the overall pressure losses by almost 50%. For a typical coal fired steam power plant with a power output of 800 MW this results in a performance increase of roughly 300 kW.

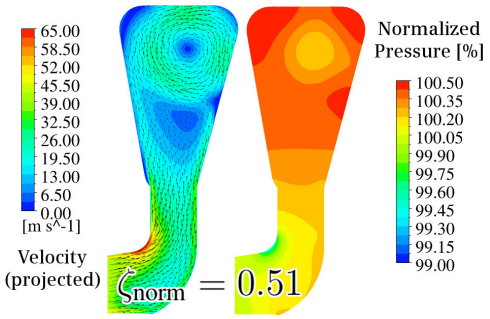

Figure 19. Velocity and pressure field for optimised design.

3. Discussion

In the present study, a numerical model of a typical high-pressure turbine exhaust section is presented and validated with a fair amount of experimental data. The $k - \omega$ turbulence model is chosen as it best fit the experimental data, although any of the investigated eddy viscosity turbulence models are able to predict the main flow phenomena. This numerical model is used in a parameter study to evaluate the main geometric parameters of the ring chamber cross-section influencing the performance of the turbine exhaust. The main findings can be summarized as follows:

- It could be shown that sharp corners and therefore a rectangular cross-section is advantageous over a round cross-section, as the stagnant flow in the corners leads to additional drag forces and thus lower rotational velocity of the ring vortex.
- A negatively inclined wall in flow direction at the diffuser exit leads to an increased diffusion and therefore lower flow losses.
- A large aspect ratio h/w of the ring chamber cross-section leads to lower flow losses due to increased diffusion and a smaller ring vortex.

With a combination of those findings the flow losses could be reduced by almost 50% compared to the baseline design with a quadratic cross-section. Thus, the findings presented in this paper allow for a qualitative assessment of the performance differences for various designs without the need for expensive CFD simulations.

Acknowledgments: The authors gratefully acknowledge Siemens AG for their support and permission to publish this paper. The responsibility for the contents lies solely with its authors.

Author Contributions: Christian Musch and Ruben Steinhoff conceived the numerical setup and performed the simulations for the validation; Christian Musch, Simon Hecker and Daniel Gloss conceived the parametric model, performed the simulations for the parameter study and analyzed the data; Christian Musch wrote the paper.

Conflicts of Interest: The authors declare no conflict of interest.

Appendix A. Simulation Results for Exhaust Model 2

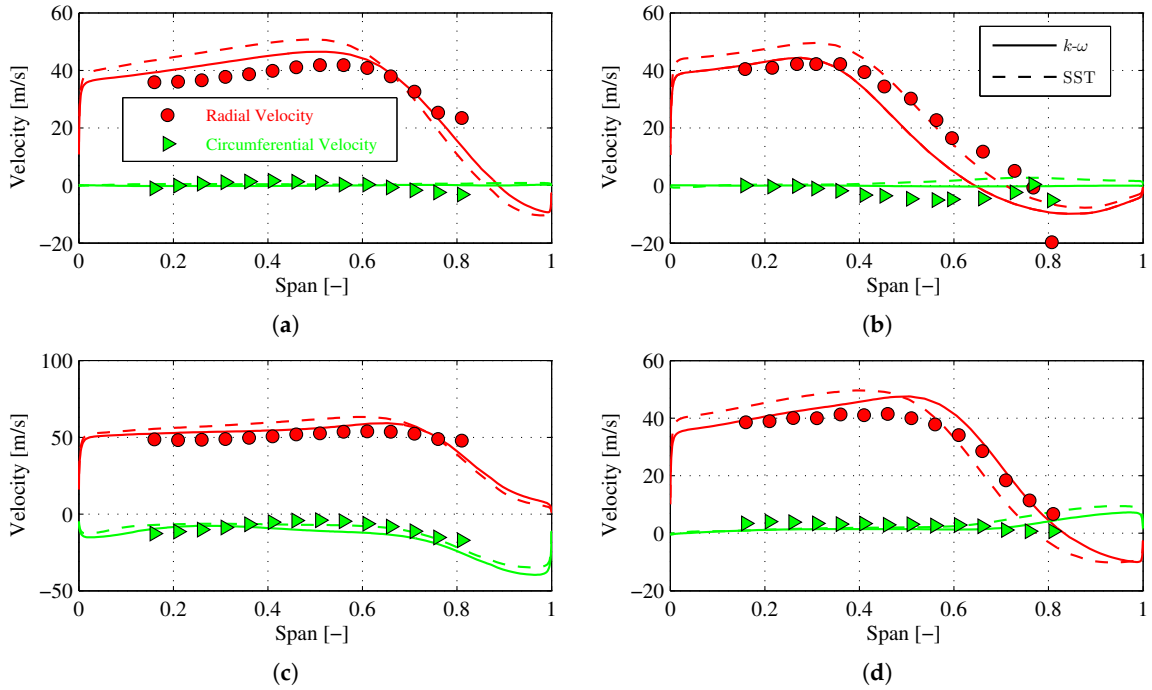

Figure A1. Velocity profiles at diffuser outlet for model 2. (**a**) Pos.1; (**b**) Pos.5; (**c**) Pos.6; (**d**) Pos.8.

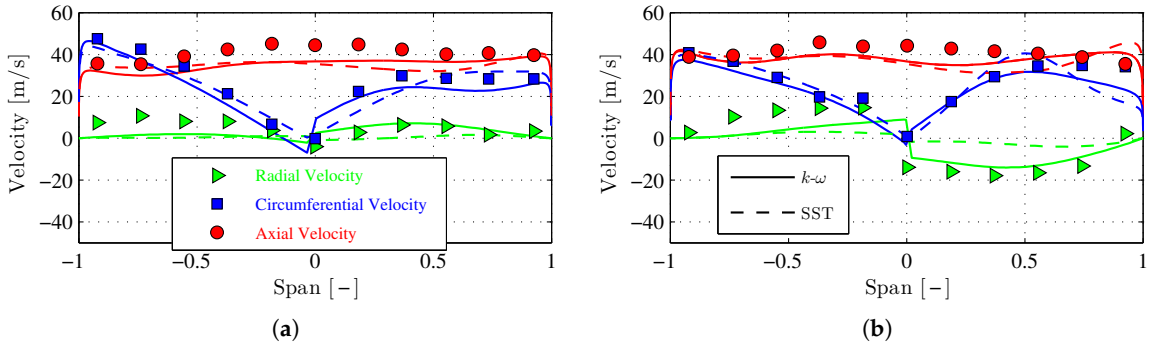

Figure A2. Velocity profiles at exhaust port for model 2. (**a**) Line 3; (**b**) Line 4.

References

1. Traupel, W. *Thermische Turbomaschinen*, 3rd ed.; Springer: Berlin–Heidelberg, Germany, 1988.
2. Hausenblas, H. Versuche an Abströmgehäusen thermischer Turbomaschinen. *Konstruktion* **1963**, *15*, 492–494.
3. Hübl, H.P. *Beitrag zur Berechnung des Spiralgehäuses von Radialverdichtern und Vorherbestimmung seines Betriebsverhaltens*; Mitteilung des Instituts für Dampf- und Gasturbinen, Technical University Vienna: Vienna, Austria, 1975; Number 7, p. 122 et sqq.
4. Lendorff, B.; Meienberg, H. Detail-Entwicklung im Bau von Turboverdichtern. *Escher Wyss Mitt.* **1944**, *17/18*, 60–67.
5. Mishina, H.; Gyobu, I. Performance investigations of large capacity centrifugal compressors. In Proceedings of the ASME International Gas Turbine Conference, London, UK, 9–13 April 1978; 78-GT-3.
6. Stiefel, W. Experiences in the development of radial compressors. In *Lecture Series 50: Advanced Radial Compressors*; von Karman Institute for Fluid Dynamics: Sint-Genesius-Rode, Belgium, 1972.
7. Ayder, E. Experimental and Numerical Analysis of the Flow in Centrifugal Compressor and Pump Volutes. Ph.D. Thesis, von Karman Institute for Fluid Dynamics, Sint-Genesius-Rode, Belgium, 1993.

8. Brown, W.B.; Bradshaw, G.R. *Design and Performance of Family of Diffusing Scrolls with Mixed-Flow Impeller and Vaneless Diffuser*; Technical Report 936; NACA: Washington, DC, USA, 1949.
9. Yang, S.; Kong, F.; Chen, B. Research on pump volute design method using CFD. *Int. J. Rotating Mach.* **2011**, *2011*, 137860.
10. Reunanen, A. Experimental and Numerical Analysis of Different Volutes in a Centrifugal Compressor. Ph.D. Thesis, Lappeenranta University of Technology, Lappeenranta, Finland, 2001.
11. Urban, M. *Experimentelle Strömungsuntersuchungen an Modellen von HD-Abströmgehäusen*; Internal Report; Siemens: München, Germany, 1997.
12. Kuwamura, Y.; Matsumoto, K.; Uehara, H. Development of new high-performance labyrinth seal using aerodynamic approach. In Proceedings of the ASME Turbo Expo, San Antonio, TX, USA, 3–7 June 2013; GT2013-94106.
13. Steglich, T.; Kitzinger, J.; Seume, J.; Van den Braembusche, R.; Prinsier, J. Improved diffuser/volute combinations for centrifugal compressors. *J. Turbomach.* **2008**, *130*, doi:10.1115/1.2749296.